Optics Letters

Multiple patterning of holographic photopolymers for increased refractive index contrast

David J. Glugla,[1,*] Madeline B. Chosy,[2] Marvin D. Alim,[3] Kimberly K. Childress,[4] Amy C. Sullivan,[1] and Robert R. McLeod[1,3]

[1]Department of Electrical, Computer, and Energy Engineering, University of Colorado Boulder, Boulder, Colorado 80309, USA
[2]Department of Chemistry, Carleton College, Northfield, Minnesota 55057, USA
[3]Materials Science and Engineering Program, University of Colorado Boulder, Boulder, Colorado 80309, USA
[4]Department of Chemical and Biological Engineering, University of Colorado Boulder, Boulder, Colorado 80309, USA
*Corresponding author: david.glugla@colorado.edu

Received 24 January 2018; revised 15 March 2018; accepted 17 March 2018; posted 19 March 2018 (Doc. ID 315104); published 12 April 2018

We demonstrate that multiple exposures of a two-component holographic photopolymer can quadruple the refractive index contrast of the material beyond the single-exposure saturation limit. Quantitative phase microscopy of isolated structures written by laser direct-write lithography is used to characterize the process. This technique reveals that multiple exposures are made possible by diffusion of the chemical components consumed during writing into the previously exposed regions. The ultimate index contrast is shown to be limited by the solubility of fresh components into the multiply exposed region.

OCIS codes: (110.0110) Imaging systems; (120.0120) Instrumentation, measurement, and metrology; (160.0160) Materials.

https://doi.org/10.1364/OL.43.001866

Direct laser writing (DLW) into photosensitive media is a common technique for fabricating embedded phase structures such as waveguides [1,2] and aperiodic volume optics [3]. Because the achievable refractive index contrast (Δn) within these materials limits features such as the minimum waveguide bend radius, or the diffraction efficiency and overall size of diffractive structures, considerable effort has gone towards the development of such photosensitive materials with increased dynamic range. Two-component photopolymers are a popular material platform for DLW of phase structures due to their high achievable Δn, ease of processing, and wide range of optical and mechanical properties [4,5]. In these materials, Δn is created through a photo-induced concentration gradient between typically high-refractive index photopolymerizable monomeric species and the low-refractive index binder/matrix. However, the primary focus on the development of these materials has been directed towards applications such as holography, data storage, and displays for augmented reality, with characterization of the total dynamic range based on M/# measurements [6] and the formula limit [4]. These metrics specify the total Δn that can be achieved using sinusoidal exposure patterns while under the assumption that only the local monomer concentration can be polymerized. However, in making this assumption, any additional contribution to the Δn from diffusion of external monomer into the exposed region is lost. Although reasonable for large area exposures and materials with low monomer diffusivity, structures such as waveguides, whose diameters are on the order of 10's of micrometers, can leverage this in-diffusion from the unexposed bulk to achieve considerably higher Δn's through multiple patterning steps.

With the advent of two-photon polymerization and the ability to fabricate micrometer-scale 3D embedded optical elements through DLW, increased effort has been invested towards characterizing the total achievable Δn and shape of these isolated structures within a photosensitive material [7–9]. Additionally, techniques such as quantitative phase imaging have been applied towards measuring the in-diffusion of monomer into the exposed region [10]. However, all of these studies were limited to investigating the results of single exposures, and neglected the replenishment of the writing monomer through post-exposure diffusion. Other investigations into the effects of multiple exposures on the resulting refractive index profile either provide only qualitative evidence of increased Δn via phase contrast microscopy [11], or consider only the total accumulated dose, ignoring the effects of in-diffusion of monomer [12]. Thus, the primary methodology for increasing the total dynamic range of two-component photopolymers has been optimization of the material chemistry [6,13,14]. This is typically difficult and/or penalized by other performance metrics such as shrinkage.

In order to extend the dynamic range of two-component photopolymers for the fabrication of isolated, micrometer-scale phase structures, we quantitatively explore the use of subsequent time-delayed photo exposures in conjunction with diffusion-assisted monomer replenishment after each exposure. We show that the total dynamic range can be increased by as much as four times the single-exposure limit in the demonstration photopolymer. Furthermore, this technique can be used to infer the maximum Δn achievable within a given two-component photopolymer, allowing for rapid screening to determine the most effective combinations of monomer

and matrix components. This multi-write technique should be beneficial in extending the utility of already-available two-component photopolymers, and allow for the fabrication of a wider range of waveguide devices and isolated optical structures.

The two-component photopolymer used in the following experiments was prepared according to a previously reported procedure [9]. Briefly, the photo-active chemistry consists of a 1:10 molar ratio of the photoinitiator TPO (2,4,6-trimethylbenzoyl-diphenyl-phosphineoxide) to a synthesized triacrylate writing monomer [phosphorothioyltris(oxybenzene-4,1-diylcarbamoyloxyethane-2,1-diyl)triacrylate]. This photoactive component was then combined in different weight fractions with the polyurethane matrix, which contained a 1:1 molar ratio of trifunctional polyisocyanate (Desmodur N3900) and difunctional polyol (polycaprolactone-block-polytetrahydrofuran-block-polycaprolactone). The material was cast between a microscope slide and coverslip, with the layer thickness set by 25 μm spacers.

The experimental setup shown in Fig. 1 was used to expose the photopolymer samples. Two lasers with wavelengths at 405 nm and 660 nm are co-aligned and focused onto the sample, which is mounted on a five-axis motorized stage. Only the 405 nm laser has sufficient spectral overlap with the photoinitiator's absorption spectrum to induce significant polymerization, allowing the 660 nm beam to be used in a confocal reflection modality. During the exposure step, a Nikon objective, operating at a numerical aperture (NA) of 0.023, provides a focused spot with a 1/exp(2) diameter of 18 μm. Because the material absorbance is 0.04 for samples with 30 wt. % of the writing monomer, and the Rayleigh range of the focused spot is 10 times larger than the thickness of the sample, the exposure profile is considered uniform throughout the polymer thickness. A Uniblitz VS14 shutter controls the exposure time.

Measurement of the refractive index profile of the written phase structures is performed using quantitative phase imaging (QPI) based on the transport of intensity equation (TIE). The procedure for performing QPI is further described in [9] and has been used to measure single-exposure conditions in the same material. The axial intensity derivative used to solve the TIE was computed using brightfield images defocused by ±3 μm about the in-focus image plane [Fig. 2(a) inset]. In order to calculate Δn from the optical path length measured using TIE, the confocal reflection microscope is used to locally measure the thickness of the polymer layer. In this case, the Nikon objective is swapped with a 0.66 NA Leica objective. A pinhole with a diameter of 1 Airy unit is used to achieve an axial resolution of 3 μm. The confocal reflection signal is fit to measure thickness with an uncertainty of ±2.5%. The unexposed polymer refractive index required to calculate the physical thickness from the confocal reflection signal is measured using a Metricon Model 2010 prism coupler.

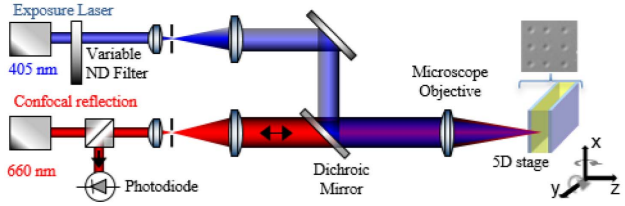

Fig. 1. Confocal reflection microscope (660 nm path) is used to position and measure the sample thickness, while the co-aligned 405 nm laser is used to expose the photopolymer and create phase structures (inset shows an example differential interference contrast microscopy image). The 660 nm laser is a 100 mW Coherent OBIS LX diode laser, and the 405 nm laser is a Power Technology Incorporated IQu2A105/8983 105 mW laser.

The multi-write technique was performed as follows: grids of spots were exposed into samples of photopolymer containing 10, 20, and 30 weight percent (wt. %) of the writing chemistry. Each spot in the grid was patterned with 316 mW/cm^2 light at a sufficient dose to consume the local monomer and saturate the photopolymer's Δn response. In this case, the dose per exposure was 253 mJ/cm^2 for the 10 wt. % samples, and 111 mJ/cm^2 for the 20 wt. % and 30 wt. % samples. After each exposure, monomer and photoinitiator were allowed to diffuse from outside the exposed region for 2 h before re-exposure. Up to 11 consecutive exposures were performed on a given spot under the same exposure conditions. Despite the long diffusion times, heating the polymer can improve monomer mobility and increase diffusivity. Figure 2(a) shows the peak Δn of the resulting refractive index structure as a function of exposure number, while a selection of the corresponding cross sections is given by Fig. 2(b). Each data point represents the average of three separate structures.

In the photopolymer formulations, up to a 4× amplification of the measured Δn beyond the single-exposure saturation limit was achieved, with peak Δn's reaching up to ∼0.03. Although the single-exposure saturation Δn increases monotonically with the initial monomer concentration [Fig. 2(a)], the maximum

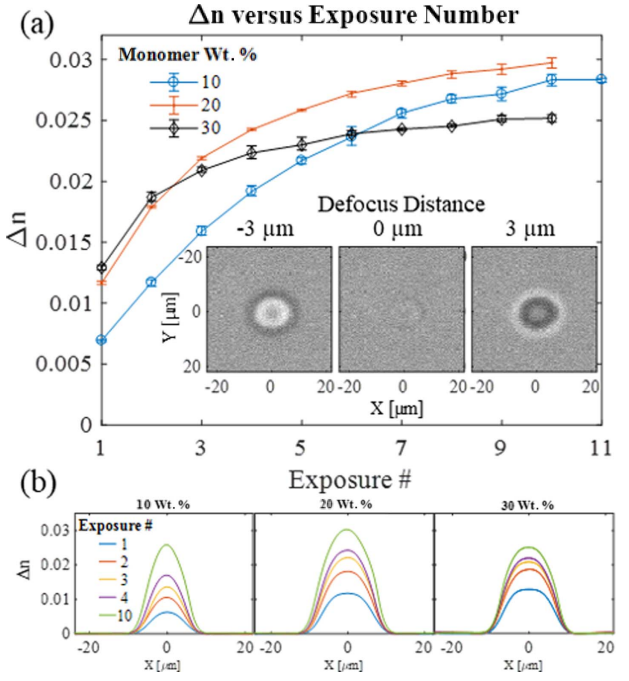

Fig. 2. (a) Peak Δn as a function of exposure number for the photopolymer with 10 wt. %, 20 wt. %, and 30 wt. % of the writing chemistry. The dose for each exposure was 253 mJ/cm^2 for the 10 wt. % samples, and 111 mJ/cm^2 for the 20 wt. % and 30 wt. % samples. Exposure intensity was 316 mW/cm^2. Each exposure occurred 2 h after the previous. The inset shows the defocused brightfield images of one of the exposed structures. (b) Δn cross sections at select exposure numbers as measured through QPI.

Δn achieved through the multi-write scheme does not exhibit a clear trend with the initial monomer loading. In general, the gain with subsequent exposures falls more rapidly at the highest monomer loadings, resulting in an overall lower multiple-exposure response.

We consider two hypotheses to explain this trend. Because Δn in holographic photopolymers is primarily due to the transport of species with contrasting refractive indices, the reduced Δn saturation limit between each new exposure indicates decreasing capability for mass transport. This decrease could be due to reduced mobility, or a solubility limit. To test the first hypothesis, QPI was used to measure the monomer diffusion time into the exposed region. To obtain an estimate for this diffusivity, the photopolymer is initially patterned using a single exposure dose, such that a large fraction of the local monomer is converted into polymer [see the $t = 0$ min profiles in Figs. 3(a) and 3(b)]. Due to the resulting concentration gradient, new monomer diffuses into the exposed region [$t > 0$ min profile in Fig. 3(a)]. During this diffusion, a delayed, identical exposure converts any replenished monomer to polymer. This new polymer adds to that from the initial $t = 0$ min exposure to generate the corresponding $t > 0$ min profiles in Fig. 3(b). After this last exposure, monomer is allowed to re-equilibrate before performing QPI. Since concentration is directly proportional to Δn for dilute solutions under the Lorentz-Lorenz model, QPI enables direct measurement of diffusion [15]. Here, Δn obtained for the $t = 0$ min delay acts as the baseline, i.e., no in-diffused monomer. The Δn profiles obtained for $t > 0$ min exposure delays are compared to this baseline to determine the concentration of in-diffused monomer. Then, monomer diffusivity is determined by fitting the time-dependent profile to a circularly symmetric 2D Fickian diffusion model. For a photopolymer with initial conditions given by (1), (2), and (3), where the initial spatial concentration of monomer within the circularly symmetric exposure region bounded by $r \le a$ is given by $C(r < a) = f(r)$ at time $t = 0$, the solution to the Fickian diffusion equation is given by (4). The concentration of monomer at the boundary of the exposed region is assumed to remain constant at $C = C_o$, and the initial distribution of monomer $f(r)$ is a saturated Gaussian, which is dependent on the exposure beam waist ω_o, the measured Δn, and the saturation level Δn_{sat}. From this solution, the average monomer diffusivity D into the exposed region can be determined:

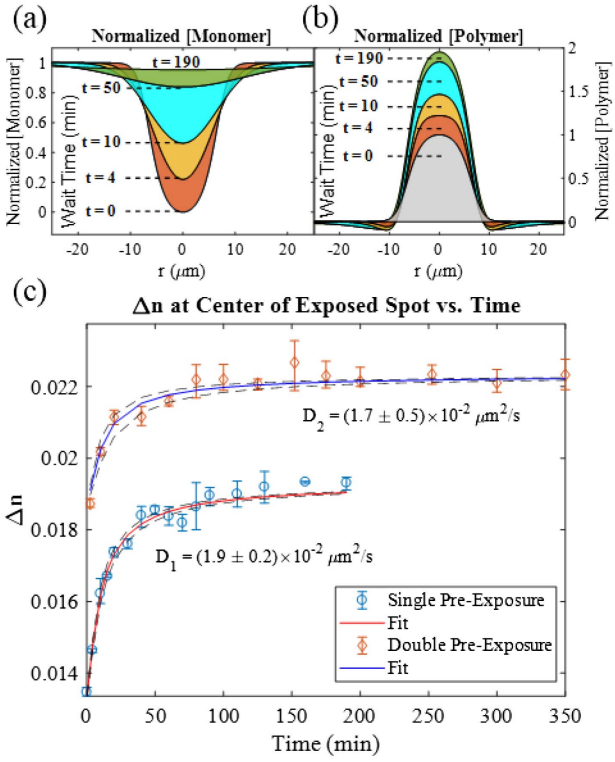

Fig. 3. (a), (b) Theoretical profiles computed using (4) and the measured diffusivity, which serve to demonstrate the measurement of monomer diffusion time. After the bleaching exposure at time $t = 0$, monomer is locally depleted and converted to polymer. Replacement monomer then diffuses from the surrounding unexposed region. Performing a second delayed exposure polymerizes and immobilizes the in-diffused monomer. After re-equilibration of the remaining monomer, this excess of high-refractive index species results in a Δn that can be measured using phase imaging. (c) Resulting fits to extract the monomer diffusivity in a sample with 30 wt. % writing chemistry after a single pre-exposure and two pre-exposures. The black dashed lines represent the confidence interval for the diffusivity fit.

$$C = C_0, \qquad r = a, \quad t \le 0, \tag{1}$$

$$C = f(r), \qquad 0 < r < a, \quad t = 0, \tag{2}$$

$$f(r) = C_0\left(1 - \frac{1}{\frac{1}{\Delta n \times \exp\left(-2\frac{r^2}{a_0^2}\right)} + \frac{1}{n_{\text{sat}}}}\frac{\Delta n + n_{\text{sat}}}{\Delta n n_{\text{sat}}}\right), \tag{3}$$

$$C = C_0\left(1 - \frac{2}{a}\sum_{n=1}^{\infty}\frac{1}{a_n}\frac{J_0(r\alpha_n)}{J_1(a\alpha_n)}\exp(-D\alpha_n^2 t)\right) + \frac{2}{a^2}\sum_{n=1}^{\infty}\exp(-D\alpha_n^2 t)\frac{J_0(r\alpha_n)}{J_1^2(a\alpha_n)}\int rf(r)J_0(r\alpha_n)\mathrm{d}r, \tag{4}$$

where $r\alpha_n$ are the zeros of the Bessel functions of the first and second kind (J_1 and J_2). Here, D is assumed to be uniform across the exposed structure, and the technique provides an averaged diffusivity after an arbitrary number of delayed writes. This allows comparisons of monomer diffusion times into the exposed region during each step of the multi-exposure process, and provides insight into the change of the local polymer network due to writing monomer polymerization. In this work, the average diffusivity after a single initial exposure and two initial exposures (separated in time by 2 h) into a sample with 30 wt. % monomer has been measured [Fig. 3(c)]. After a single pre-exposure, the measured monomer diffusivity is 1.9 $\mu m^2/s$ and does not decrease within the uncertainty of the measurement after the second pre-exposure, indicating that sufficient delay time between exposures has been achieved. Additionally, Fig. 3(c) reveals that even after equilibration of monomer, the additional Δn achieved after consecutive writes decreases relative to the first exposure. This indicates that local decreases in monomer solubility constrain the maximum refractive index obtained from multiple exposures.

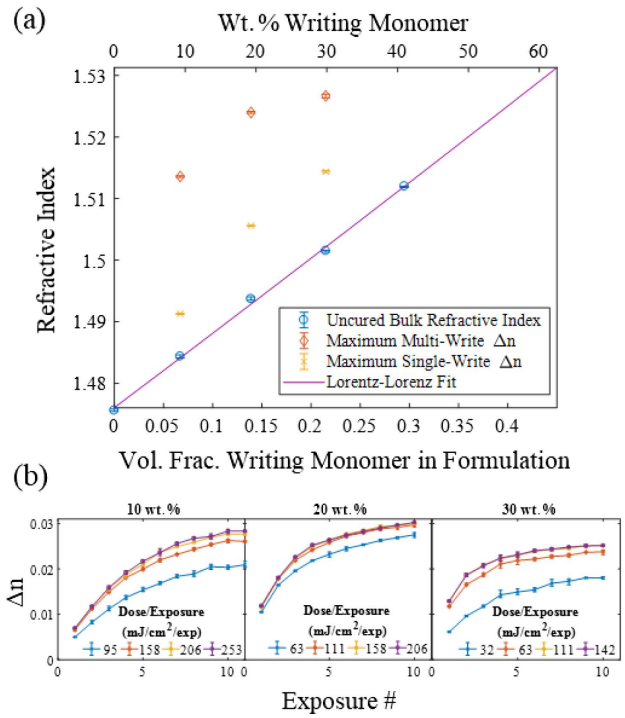

Fig. 4. (a) Background refractive index of the photopolymer and its fit to the Lorentz–Lorenz model, added to the measured Δn to show the absolute index of each exposure. Red diamonds show the maximum refractive index from multiple exposures, while the maximum refractive indices obtained after a single exposure are plotted as yellow x's. (b) Δn for materials with different initial monomer loadings plotted against exposure number and the dose per exposure. The exposure intensity was 316 mW/cm^2.

To further investigate solubility of the monomer as a function of repeat exposures, we plot the data of Fig. 2(a) as the total refractive index of each spot by adding Δn to the measured background index in Fig. 4(a). This background refractive index is measured by preparing samples of the photopolymer with 0 wt. %, 10 wt. %, 20 wt. %, 30 wt. %, and 40 wt. % of the writing chemistry, and then performing prism coupling at 632.8 nm. Assuming that the exposed structures are sufficiently small and isolated, such that the in-diffusion of monomer during fabrication does not significantly deplete the surrounding monomer concentration, the total refractive index of the exposed spots is determined by adding the measured Δn of the structure to the corresponding bulk refractive index of the background. This shows that increasing the concentration of writing monomer enables a greater single-exposure Δn, but simultaneously constrains the maximum multiple-exposure Δn due to a limit on the maximum absolute refractive index, and thus photopolymer concentration. We attribute this maximum achievable photopolymer concentration, and its dependence on exposure conditions, to the crosslinked interpenetrating network (IPN) formed by the multi-functional acrylate. Further support that the maximum refractive index is locally limited by monomer solubility is given in Fig. 4(b), where the peak Δn at each initial monomer loading is plotted against exposure dose and number. This illustrates that the maximum multiple-exposure Δn is reduced as the individual dose is decreased, and thus solubility in the IPN is not simply given by local polymer concentration [16]. This hypothesis accounts for the absence of flat-topped, saturation features in the multi-exposure cross sections shown in Fig. 2(b). The non-uniform intensity profile of the Gaussian exposure beam creates a spatially varying dose, resulting in different kinetics and a non-uniform crosslink density over the multiple exposures.

In conclusion, these results reveal that the total achievable Δn for small, isolated structures depends on the interplay between the single or multiple exposure conditions, and wt. % of writing chemistry in the formulation. While it is well known that the potential refractive index change per exposure increases with monomer loading, we find competing effects of increased background refractive index and finite monomer solubility. Within these constraints, we have demonstrated the ability to achieve a four-fold enhanced refractive index contrast above the single-exposure saturation limit within two-component photopolymers without altering the initial material formulation. Additionally, the measurement technique enables the rapid study of quantities such as monomer diffusivity and solubility as a function of exposure conditions. Understanding the evolution of these limits to material response will aid in the formulation of high Δn photopolymers.

Funding. Division of Emerging Frontiers in Research and Innovation (EFRI) (1240374); National Science Foundation (NSF) (1721055, 1307918).

Acknowledgment. Parts of this work were presented at SPIE Optics + Optoelectronics (Holography: Advances and Modern Trends V) in 2017, Analysis of holographic photopolymers for integrated optical systems via quantitative phase microscopy; doi: 10.1117/12.2265873.

REFERENCES

1. A. C. Sullivan, M. W. Grabowski, and R. R. McLeod, Appl. Opt. **46**, 295 (2007).
2. G. D. Marshall, M. Ams, and M. J. Withford, Opt. Lett. **31**, 2690 (2006).
3. T. D. Gerke and R. Piestun, Nat. Photonics **4**, 188 (2010).
4. B. A. Kowalski and R. R. McLeod, J. Polym. Sci. Part B Polym. Phys. **54**, 1021 (2016).
5. J. Guo, M. R. Gleeson, and J. T. Sheridan, Phys. Res. Int. **2012**, 1 (2012).
6. K. Curtis, L. Dhar, A. J. Hill, W. L. Wilson, and M. R. Ayres, *Holographic Data Storage: From Theory to Practical Systems*, 1st ed. (Wiley, 2010).
7. A. Žukauskas, I. Matulaitienė, D. Paipulas, G. Niaura, M. Malinauskas, and R. Gadonas, Laser Photon. Rev. **9**, 706 (2015).
8. A. Jesacher, P. S. Salter, and M. J. Booth, Opt. Mater. Express **3**, 1223 (2013).
9. D. J. Glugla, M. B. Chosy, M. D. Alim, A. C. Sullivan, and R. R. McLeod, Opt. Express **26**, 1851 (2018).
10. T. Babeva, I. Naydenova, S. Martin, and V. Toal, Opt. Express **16**, 8487 (2008).
11. J. Kumpfmueller, K. Stadlmann, Z. Li, V. Satzinger, J. Stampfl, and R. Liska, Des. Monomers Polym. **17**, 390 (2013).
12. M. S. Dinleyici and C. Sümer, Opt. Commun. **284**, 5067 (2011).
13. B. A. Kowalski, A. C. Urness, M.-E. Baylor, M. C. Cole, W. L. Wilson, and R. R. McLeod, Opt. Mater. Express **4**, 1668 (2014).
14. F.-K. Bruder, T. Fäcke, and T. Rölle, Polymers **9**, 472 (2017).
15. W. Heller, J. Phys. Chem. **69**, 1123 (1965).
16. C. I. Fiedler, E. A. Aisenbrey, J. A. Wahlquist, C. M. Heveran, V. L. Ferguson, S. J. Bryant, and R. R. McLeod, Soft Matter **12**, 9095 (2016).